MR Imaging with Hyperpolarized ^{3}He Gas

Hunter Middleton, Robert D. Black, Brian Saam, Gordon D. Cates, Gary P. Cofer, Robert Guenther, William Happer, Lawrence W. Hedlund, G. Alan Johnson, Kim Juvan, John Swartz

Magnetic resonance images of the lungs of a guinea pig have been produced using hyperpolarized helium as the source of the MR signal. The resulting images are not yet sufficiently optimized to reveal fine structural detail within the lung, but the spectacular signal from this normally signal-deficient organ system offers great promise for eventual *in vivo* imaging experiments. Fast 2D and 3D GRASS sequences with very small flip angles were employed to conserve the nonrenewable longitudinal magnetization. We discuss various unique features associated with performing MRI with hyperpolarized gases, such as the selection of the noble gas species, polarization technique, and constraints on the MR pulse sequence.

Key words: MRI; gas; helium; hyperpolarized.

INTRODUCTION

The production of the first magnetic resonance (MR) images using hyperpolarized Xenon (^{129}Xe) gas (1) has introduced the possibility of a dramatic new contrast modality for MRI. Organs with air spaces, such as the lungs, and tissues with high solubilities of certain noble gas species are particularly likely candidates for the application of this new MR imaging technique. Hyperpolarized helium (^{3}He) has certain technical advantages over ^{129}Xe as an MR signal source, and we have now extended noble gas imaging by producing hyperpolarized ^{3}He images of guinea pig lungs.

The key feature of the hyperpolarized gases is the extremely large, nonequilibrium polarization in the nuclei. In fact, the nuclear polarization can be as much as 10^4 to 10^5 times greater than the equilibrium polarization of water protons in typical spectrometer magnets, easily overcoming the factor of about 10^3 loss in signal from the lower gas density. Even accounting for the different gyromagnetic ratios, the MR signal from the gas at atmospheric pressure can be more than an order of magnitude larger than that from an equal volume of water. Note that when working with hyperpolarized gases, the magnetization is independent of the applied magnetic field, so that the MR signal scales with the square of the gyromagnetic ratio.

For example, if we assume a 30% ^{3}He polarization, a value that has been achieved in large volumes (170 cc) (2), then a given volume of ^{3}He at one atmosphere will produce 10.3 times more signal than an equivalent volume of water in a 2 Tesla field (for which the polarization will be $\sim 7 \times 10^{-6}$) as can be seen in Table 1. If the ^{3}He signal is acquired in a noise background produced by biological fluids, then the sample noise will be dominated by the Johnson noise from the fluids at the ^{3}He Larmor frequency. That is, the linear dependence of sample noise on frequency (3) means less sample noise will be seen at 64 MHz (the Larmor frequency of ^{3}He at 2 T) than at 85 MHz. Thus, signal-to-noise ratio (SNR)/voxel in a ^{3}He image under the conditions stated above will be 13.5 times greater than that which would be realized in a proton scan (assuming no substantial noise from the coil and electronics).

Noble gases are particularly amenable to the creation of large, highly nonequilibrium polarizations, due primarily to the very long T_1s which can be achieved for their nuclei (4–8). Contrary to the case for conventional proton imaging, a long T_1 is vital in order to produce and preserve the nonequilibrium polarization. Long T_1s are generally possible in noble gases because the electrons in the filled orbitals of an isolated noble gas atom produce neither an electric-field gradient nor a magnetic field at their nucleus. For the nuclei of isolated, monatomic noble gases, there are also no interactions with nearby nuclear moments or molecular moments such as occur in polyatomic molecules. For these reasons, the nuclear spins of noble gases relax very slowly compared with the nuclear spins of other gases or hydrogen protons in water.

The two noble gas isotopes ^{129}Xe and ^{3}He stand out among the rest in part because they are the only nonradioactive noble gases with nuclear spins of ½. Atoms with nuclear spins greater than ½ (e.g., ^{131}Xe with spin 3/2) have a nuclear electric quadrupole moment and are therefore sensitive to torque resulting from interactions with collisionally induced electric field gradients. ^{3}He and ^{129}Xe have no electric quadrupole moment and are therefore sensitive only to the generally smaller torques exerted by collision-induced magnetic fields. Still, some isotopes with nuclear spin >½, such as ^{83}Kr and ^{21}Ne, are known to have appreciable lifetimes under certain conditions, but are extremely expensive in isotopically enriched form.

We have chosen to work with ^{3}He to explore several practical advantages it may have over ^{129}Xe, even though ^{129}Xe has some potentially unique and important characteristics (e.g., its lipophilic nature and smaller self-

MRM 33:271–275 (1995)

From the Department of Physics, Princeton University, Princeton, New Jersey (H.M., B.S., G.D.C., W.H.); and the Center for *In Vivo* Microscopy, Duke University Medical Center (R.D.B., G.P.C., L.W.H., G.A.J.), the Department of Biomedical Engineering (R.D.B.), and the Department of Physics B.G., G.A.J., K.J., J.S.), Duke University, Durham, North Carolina.

Address correspondence to: Hunter Middleton, Ph.D., Physics Department, P.O. Box 708, Princeton University, Princeton, NJ 08544–0708.

Received November 16, 1994; revised December 15, 1994; accepted December 15, 1994.

This work was supported by AFOSR grant F49620–92-J-0211, ARPA grant DAMD17–94-J-4469, ARO grant DAAH04–94-0204, NIH grant P41 RR05959, and NSF grant CDR 8622201.

0740-3194/95 $3.00

Table 1
A Comparison of Equilibrium (Boltzmann) and Nonequilibrium Signal Voltages (for Spin ½)

	Boltzmann	Nonequilibrium
Magnetization	$\frac{N\gamma\omega\hbar^2}{4k_BT}$	$\frac{N\gamma\hbar P}{2}$
NMR signal voltage (proportional)	$\frac{N\gamma\omega^2\hbar^2}{4k_BT}$	$\frac{N\gamma hP\omega}{2}$
Signal voltage ratio: Nonequilibrium (gas)-to-equilibrium (water)		$\frac{2k_BTP\omega_g\gamma_gN_g}{h\omega_p^2\gamma_pN_p}$

Where γ is the gyromagnetic ratio, ω is the Larmor frequency, P is the polarization, k_B is Boltzmann's constant, T is spin temperature, N is spin number density, and the subscripts "g" and "p" refer to gas and proton, respectively. N_g/N_p = ½₅₀₀ for gas at a pressure of 1 atmosphere.

diffusion coefficient) (1). First, the magnetic moment of ^{3}He is 2.7 times larger than that of ^{129}Xe. Given the quadratic dependence of the NMR signal voltage on magnetic moment, this leads to MR signals that are 7.6 times greater for a given polarization density. Furthermore, although ^{129}Xe can be polarized faster than ^{3}He (a few minutes versus a few hours), it also depolarizes much faster in the gas phase (tens of minutes versus tens of hours), necessitating storage in the form of an ice at liquid nitrogen temperatures or below if not used immediately (5, 6). A helium-oxygen mixture can also be breathed indefinitely (e.g., by deep sea divers) whereas xenon is a natural anesthetic with roughly a 70% minimum anesthesia concentration (9). Finally, although ^{3}He and ^{129}Xe have similar T_1s in the presence of oxygen (10), it is possible that ^{3}He will have longer lifetimes in other biologically important environments because it is more mobile and will therefore experience fluctuating magnetic fields on much shorter time scales than will ^{129}Xe.

For these first tests of MRI on hyperpolarized ^{3}He, we decided to image the lungs, traditionally a difficult organ system to image because of low water content, a short T_2, and significant susceptibility differences. Imaging a hyperpolarized gas that has been introduced into the lungs therefore provides a particularly good test of the benefits of hyperpolarized gas imaging as a complement to conventional proton MRI.

METHODS

^{3}He Polarization Process

The hyperpolarized gas is prepared using collisional spin exchange with an optically pumped alkali-metal vapor (11–13). Circularly polarized laser light tuned to the 795 nm D1 resonance in rubidium illuminates a glass ampule containing the ^{3}He gas and rubidium alkali metal. The ampule is heated to produce a rubidium vapor density of roughly 1 ppm of the ^{3}He density. Absorption of the circularly polarized laser light produces a high electronic polarization in the rubidium atoms through depopulation optical pumping. Subsequent gas collisions between the rubidium and ^{3}He then transfer some of this polarization to the ^{3}He nuclei. The collisional spin-exchange is mediated by a hyperfine interaction between the alkali valence electron and the ^{3}He nucleus, and is very slow, with typical time constants on the order of hours. However, if the glass ampules containing the gas are carefully prepared, the T_1 of the ^{3}He can be anywhere from a few tens of hours to hundreds of hours (4), which permits the creation of polarizations in excess of 50% (14).

A variety of ^{3}He ampules was used, ranging from 3.5 to 8 atm of ^{3}He, with roughly spherical volumes of 7 to 10 cc, and containing a few milligrams of rubidium metal and a few tens of mbar of nitrogen. The glass ampules were filled with the desired amount of ^{3}He, rubidium, and nitrogen on a high purity gas handling system to ensure the cleanliness necessary for long T_1s. A number of these ampules were fashioned with thin break-stems so that after being polarized the gas could be released into the guinea pig.

The optical pumping apparatus consisted of the laser system, a set of magnetic field coils, a hot air oven and a small NMR polarization measurement system. The laser system uses a 10 W commercial argon-ion laser to pump a homemade Ti:Sapphire laser with a net continuous output of 800 mW at 795 nm and a spectral width of several hundred GHz FWHM. This output is not optimal, because the absorption width of the pressure-broadened rubidium line is only around 100–200 GHz FWHM (15), but it was adequate for this first test. The oven controls the rubidium vapor pressure in the ampules and typically operates at 170°C in order to create an optically dense rubidium vapor (2.5×10^{14} cm^3) which absorbs most of the available laser power. A 5- to 10-Gauss holding field was produced by the 80-cm diameter Helmholtz magnetic field coils. The polarimetry system used adiabatic fast passage NMR to provide a relative polarization measurement.

After a sufficient polarization built up in the ^{3}He ampules, they were cooled to room temperature and carried to the MR imaging system. At room temperature the rubidium vapor condensed out on the walls of the ampule so that no rubidium vapor was introduced into the animal. Although the pumping station NMR system only provides a relative measurement of the ^{3}He polarization, calculations using the previously measured spin-exchange rate constant (4) indicated that the ^{3}He polarization was between 5% and 20% when the optical pumping was stopped. Each ampule required 4 to 8 h to polarize to this level.

Polarized Gas Transfer

For delivery of the hyperpolarized gas to the guinea pig (400–450 g), we first anesthetized the animals with intraperitoneal injections of nembutal (40 mg/kg) and butorphanol (3 mg/kg), and also injected them with atropine sulfate (0.35 mg/kg). A 3.5-cm long 14 gauge intracatheter was inserted into the trachea, and 3–0 silk ligatures were tied around the endotracheal tube to provide a gas tight path to the lungs. The animal was then secured in a plexiglas cradle and placed in the detector coil. Just prior to being connected to the polarized gas delivery system, the animal was euthanized with an

overdose of nembutal (85 mg/kg, intraperitoneally), and a laporotomy incision was made just below the rib cage. The diaphragm was exposed and cut to deflate the lungs. The endotracheal tube was then connected by a 10-cm length of flexible hose to the break-stem of the polarized ^{3}He ampule. The flexible hose was bent by hand, cracking the break-stem and allowing the gas to flood the lungs of the guinea pig. The ^{3}He ampules initially contained 3.5 atm of ^{3}He with an 8-cm^3 volume, so that when broken, about 20 cm^3 of gas was introduced into the lungs. As soon as the ampule was broken, the imaging sequence was begun. The elapsed time between breaking open the ampule and beginning the imaging sequence was only a few seconds.

MR Spectrometer System

All images were acquired on a 2-Tesla, 30-cm horizontal Omega CSI magnet (G.E. NMR Instruments, Fremont, CA) with shielded coils capable of producing gradients to 18 Gauss/cm. The RF coil was an 8-cm "birdcage" design, tuned to the ^{3}He frequency (~65 MHz). One of the modes of this coil supports a resonance near the proton frequency of 85 MHz, which allowed alignment of the desired slice before the gas was introduced (even though one portion of the proton image was obscured due to the inhomogeneous RF field). The gradient and RF system are controlled by a General Electric Signa (version 5.4) console, which is interfaced to the RF system by an intermediate frequency mixer.

Images were acquired using 2D and 3D GRASS pulse sequences. Small flip angles were used to ensure a relatively constant magnetization during the acquisition of a given image. For hyperpolarized gas, the magnetization remaining after n excitations, assuming uniform excitation of the entire sample and no environmental T_1 decay, is simply $(\cos \alpha)^n$ where α is the flip angle. Thus, it is easy to calculate the flip angle to be used for a given ending value of magnetization.

RESULTS

Guinea Pig Lung Images

Figure 1 shows a series of ^{3}He images of the lung and mid-chest level in a 400-g guinea pig. The desired axial position in the lungs was found with a proton locator scan. Hyperpolarized gas was then introduced and successive scans of the same 2D slice were run until no significant longitudinal magnetization remained. The 2D GRASS sequence used a flip angle of roughly 6°, and specified a slice thickness of 10 mm with a 72-mm field of view covered by a 128 × 256 matrix. The 2.1-ms *TE* and 11-ms *TR* yielded a scan time of 1.41 s. Delays between images were such that one image was acquired every 4 s. Over a 3.5-min period, 48 individual scans were taken, and the last image still had an observable signal. With 128 excitations/slice, each 2D scan reduced the polarization in the slice by 50%. However, there was presumably replenishment by diffusion from unexcited, adjacent regions of the sample. The images shown are samples at 8-s intervals (every other image in the first part of the series).

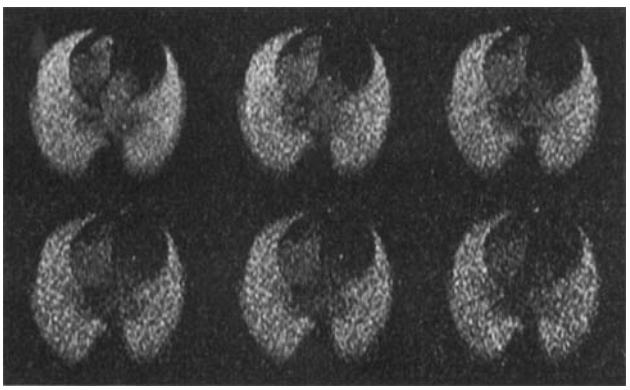

FIG. 1. Time sequence of axial ^{3}He images acquired with a GRASS sequence (*TE* = 2.1 ms, *TR* = 11 ms) in a guinea pig lung. The time interval between images is 8 s.

Figure 2 is a comparison of the ^{3}He image (Fig. 2a) to a proton image (Fig. 2b) taken in a separate experiment with a live animal to provide anatomic landmarks. The ^{3}He image was generated by summing the first four images in the time course series to improve the SNR. Due to the large volume of gas delivered, He escaped into the heart, as is evident in the first image of the time course (Fig. 1) and in Fig. 2a.

A 3D GRASS sequence was then performed with a different animal. For this run, the gas delivery system was modified to include a "T" connector with a small polyethylene bag to reduce the volume of gas delivered to the lungs. The flip angle was reduced to 2° and a 32 × 128 × 256 matrix was acquired. The field of view was 62 mm with a 15.6-mm total slice thickness. Data were zero-filled (along the phase encode direction), yielding voxels of 0.24 × 0.24 × 0.5 mm. The resulting array was interpolated along the z-axis to produce cubic voxels. Figure 3 shows two different views of the data volume rendered on a Silicon Graphics Reality Engine (Silicon Graphics Inc., Mountainview, CA) using VoxelView Ultra software (Vital Images, Inc., Fairfield, IA). Figure 3a is most closely equivalent to an anteroposterior (frontal) view, while Fig. 3b is an oblique perspective. Left and right lungs are seen with a signal void in the region of the mediastinum.

DISCUSSION

Although dramatic, the results presented here are far from being optimized. The available signal from the ^{3}He gas can be increased further and more efficient pulse sequences can be designed.

MRI with hyperpolarized gases presents a unique challenge in selecting a proper pulse sequence. Because the nuclear polarization is in a highly nonequilibrium state, every excitation depletes polarization that cannot be recovered by waiting for a return to equilibrium. On the other hand, there is also no recovery time needed between excitations. Thus, high speed techniques with low, variable flip angles or multiple echoes (e.g., GRASS, FLASH, and echo planar) are applicable and attractive, both for their speed and their efficiency in using the available magnetization. The long T_2s necessary for multiple-echo sequences may be possible given the absence

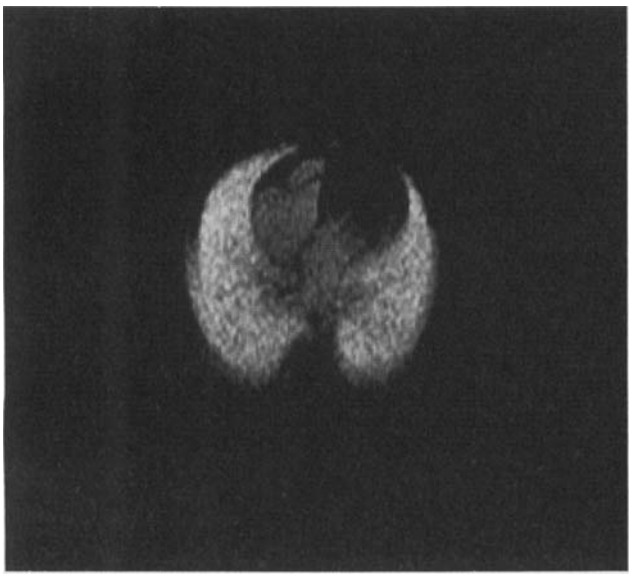

a

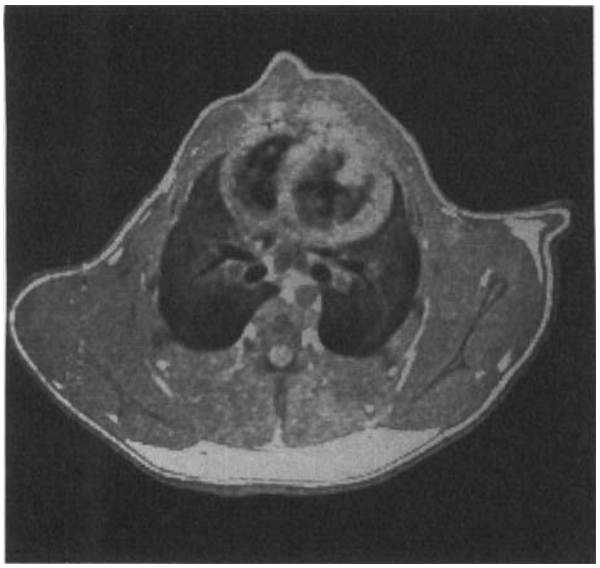

b

FIG. 2. (a) The first four images of the time series shown in Fig. 1 have been averaged together to improve the SNR. (b) Axial ^{1}H images of a different animal show the proton anatomy.

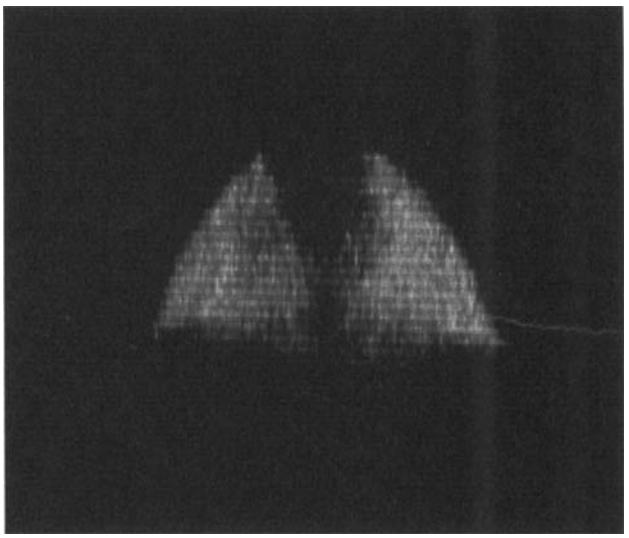

a

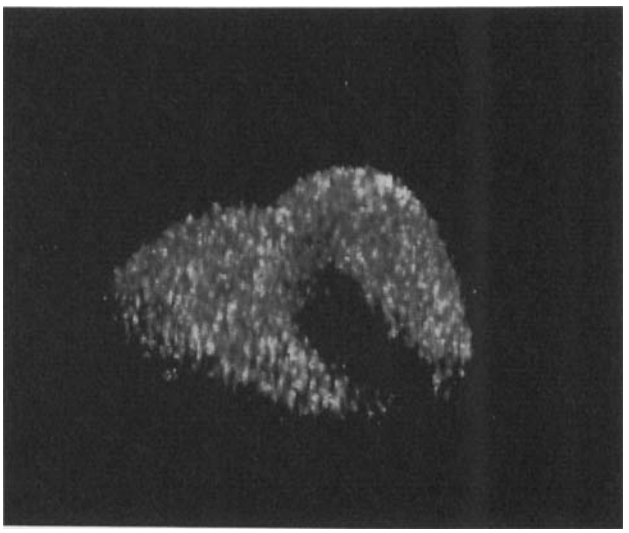

b

FIG. 3. Volume rendering was employed to generate different perspectives of the 3D data set: (a) frontal (AP) view, and (b) oblique view.

of significant dipole-dipole relaxation in the gas phase. Very short *TE*s may also reduce any diffusion-related image artifacts resulting from gas diffusion constants on the order of 1 cm^2/s. More definitive statements on useful pulse sequences will need to await further exploration of the relaxation properties of the gas *in vivo* and the magnitude of any diffusion effects.

A detailed discussion of the effects of diffusion is beyond the scope of this paper. However, we note that diffusion plays a prominent role in MR microscopy where the voxel dimensions are comparable with the diffusion path length during acquisition. The impact on signal and the point spread function have been discussed by several authors (16–20). The advent of a signal source with a diffusion coefficient several orders of magnitude higher than that of protons in tissues clearly poses some fascinating problems and potentials.

Previous experience with hyperpolarized gases indicates that much higher ^{3}He polarizations and volumes are possible. Controlled experiments with small sample volumes (7 cc and 8 atm) have demonstrated polarizations of up to 65% (14). Perhaps more applicable to the present work, polarizations of 30–40% have been accomplished in 170 cc, 8 atm samples of ^{3}He under less than ideal conditions (2), so that it is reasonable to expect the results to be reproducible. In this MRI work, the long T_1 ^{3}He gas ampules were prepared using the same techniques that were crucial to the earlier results. The other primary requirement for achieving high polarizations is the use of higher-power lasers during the optical-pump-

ing stage. These lasers are currently available commercially and could be easily incorporated into our optical pumping system.

To facilitate more rapid research on the capabilities of gas imaging, we believe that a reusable system for producing larger volumes of hyperpolarized gas is also an important next step. Although the use of break-stem ampules was successful in these first tests, overall it is a very inefficient and cumbersome mechanism for getting hyperpolarized gas into animal lungs. We are now planning a continuous polarized gas delivery system that will enable ventilation of a live animal in a cardiac-gated experiment.

In addition to *in vivo* microscopy research with small animals, we believe that application of the hyperpolarized gas MRI technology to clinical work should be pursued. Hyperpolarized gases offer the unique possibility of introducing an MR signal agent into systems that are signal-deficient or even tracking a transient build-up signal in studies of transport processes. The most likely candidates for such work are organ systems with open gas volumes and tissues with high solubilities of either ^{3}He or ^{129}Xe.

For example, helium has roughly the same saturation in all tissue types (1% of the local gas density (21)). The chemical shift realized by helium gas when dissolved in water is only about 0.3 ppm (22). The Dixon technique (23) might still be used to acquire separable images of gas transport to the blood, suggesting that inert gas imaging may develop into a very powerful tool for ventilation-perfusion scans. One might also make use of the large change in diffusion coefficient in going from the free-gas state to the dissolved gas state to dephase the free gas component, thereby leaving only the dissolved gas signal. Furthermore, tracing polarized gas in the blood may also provide a unique contrast enhancement because the gas is a signal source as opposed to a relaxation agent.

Many questions remain about the polarization lifetime of hyperpolarized gases in blood and tissues. Yet the robustness of the polarized gas we have observed in guinea pig lungs and the relative ease with which it has been applied in these exploratory imaging experiments is very encouraging for its potential in MRI.

ACKNOWLEDGMENTS

The authors thank B. Driehuys for many useful discussions, M. Souza for technical assistance, and E. Fitzsimons for editorial assistance.

REFERENCES

1. M. Albert, G. Cates, B. Driehuys, W. Happer, B. Saam, C. J. Springer, A. Wishnia, Biological magnetic resonance imaging using laser-polarized ^{129}Xe. *Nature* **370,** 199–201 (1994).
2. P. Anthony, R. Arnold, H. Band, H. Borel, P. Bosted, V. Breton, G. Cates, T. Chupp, F. Dietrich, J. Dunne, R. Erbacher, J. Fellbaum, H. Fonvieille, R. Gearhart, R. Holmes, E. Hughes, J. Johnson, D. Kawall, C. Keppel, S. Kuhn, R. Lombard-Nelsen, J. Marroncle, T. Maruyama, W. Meyer, Z.-E. Meziani, H. Middleton, J. Morgenstern, N. Newbury, G. Petratos, R. Pitthan, R. Prepost, Y. Roblin, S. Rock, S. Rokni, G. Shapiro, T. Smith, P. Souder, M. Spengos, F. Staley, L. Stuart, Z. Szalata, Y. Terrien, A. Thompson, J. White, M. Woods, J. Xu, C. Young, G. Zapalac, Determination of the neuron spin structure function. *Phys. Rev. Lett.* **71,** 959–962 (1993).
3. R. D. Black, T. A. Early, P. B. Roemer, O. M. Mueller, A. Morgo-Campero, L. G. Turner, G. A. Johnson, A high temperature superconducting receiver for NMR microscopy. *Science* **259,** 793–795 (1993).
4. N. Newbury, A. Barton, G. Cates, W. Happer, H. Middleton, Gaseous ^{3}He - ^{3}He magnetic dipolar spin relaxation. *Phys. Rev. A* **48,** 4411–4420 (1993).
5. M. Gatzke, G. Cates, B. Driehuys, D. Fox, W. Happer, B. Saam, Extraordinarily slow nuclear spin relaxation in frozen laser-polarized ^{129}Xe. *Phys. Rev. Lett.* **70,** 690–693 (1993).
6. G. Cates, D. Benton, M. Gatzke, W. Happer, K. Hasson, N. Newbury, Laser production of large nuclear-spin polarization in frozen xenon. *Phys. Rev. Lett.* **65,** 2591–2594 (1990).
7. S. Schaefer, G. Cates, W. Happer, Determination of spin-exchange parameters between optically pumped rubidium and ^{83}Kr. *Phys. Rev. A* **41,** 6063–6070 (1990).
8. T. Chupp, K. Coulter, Polarization of ^{21}Ne by spin exchange with optically pumped Rb vapor. *Phys. Rev. Lett.* **55,** 1074–1077 (1985).
9. H. Luttropp, G. Rydgren, R. Thomasson, O. Werner, A minimal flow system for Xe anesthesia. *Anesthesiology* **75,** 896–902 (1991).
10. C. Jameson, A. Jameson, J. Hwang, Nuclear spin relaxation by intermolecular magnetic dipole coupling in the gas phase. *J. Chem. Phys.* **89,** 4074–4081 (1988).
11. M. Bouchiat, T. Carver, C. Varnum, Nuclear polarization in ^{3}He gas induced by optical pumping and dipolar spin exchange. *Phys. Rev. Lett.* **5,** 373–377 (1960).
12. W. Happer, E. Miron, S. Schaefer, D. Schreiber, W. Wijngaarden, X. Zeng, Polarization of the nuclear spins of noble-gas atoms by spin exchange with optically pumped alkali-metal atoms. *Phys. Rev. A* **29,** 3092–3110 (1984).
13. T. Chupp, M. Wagshul, K. Coulter, A. McDonald, W. Happer, Polarized high-density gaseous *^{3}He targets. Phys. Rev. C* **36,** 2244–2251 (1987).
14. N. Newbury, A. Barton, P. Bogorad, G. Cates, M. Gatzke, B. Saam, L. Han, R. Holmes, P. Souder, J. Xu, D. Benton, Laser polarized muonic helium. *Phys. Rev. Lett.* **67,** 3219–3222 (1991).; erratum, *Phys. Rev. Lett.* **69,** 391 (1992).
15. C. Ottinger, R. Scheps, G. York, A. Gallagher, Broadening of the Rb resonance lines by the noble gases. *Phys. Rev. A* **11,** 1815–1828 (1975).
16. B. Putz, D. Barsky, K. Schulten, Edge enhancement by diffusion: microscopic magnetic resonance imaging of an ultrathin glass capillary. *Chem. Phys.* **183,** 391–396 (1991).
17. Z. H. Cho, C. B. Ahn, S. C. Juh, H. K. Lee, R. E. Jacobs, S. Lee, J. H. Yi, J. M. Jo, NMR Microscopy with 4 μm resolution—theoretical study and experimental results. *Med. Phys.* **15,** 815–823 (1988).
18. P. T. Callaghan, C. D. Eccles, Diffusion-limited resolution in nuclear magnetic resonance microscopy. *J. Magn. Reson.* **78,** 1–8 (1988).
19. W. B. Hyslop, P. C. Lauterbur, Effects of restricted diffusion on microscopic NMR imaging. *J. Magn. Reson.* **94,** 501–510 (1991).
20. E. McFarland, Time independent point-spread function for MR microscopy. *Magn. Reson. Imaging* **10,** 269–278 (1992).
21. P. Weathersbee, L. Homer, Solubility of inert gases in biological fluids and tissues. *Undersea Biomed. Res.* **7,** 277–296 (1980).
22. R. Seydoux, P. Diehl, R. K. Mazitov, J. Joskisaari, Chemical Shifts in Magnetic Resonance of the 3 He Nucleus in Liquid Solvents and Comparison with other Noble Gases, *J. Mag. Reson.* **101,** 78–83 (1993).
23. W. T. Dixon, Simple proton spectroscopy imaging. *Radiology* **153,** 189–194 (1984).